ACS chemical biology

Articles

Cite This: ACS Chem. Biol. 2018, 13, 200−206

Expanding the Bioactive Chemical Space of Anthrabenzoxocinones through Engineering the Highly Promiscuous Biosynthetic Modification Steps

Xianyi Mei,[†,§,∥] Xiaoli Yan,[§,∥] Hui Zhang,[§] Mingjia Yu,[§] Guangqing Shen,[§] Linjun Zhou,[§] Zixin Deng,[§] Chun Lei,[*,‡] and Xudong Qu[*,†,§]

[†]School of Perfume and Aroma Technology, Shanghai Institute of Technology, Shanghai 201418, China

[‡]School of Pharmacy, Fudan University, Shanghai 201203, China

[§]Key Laboratory of Combinatorial Biosynthesis and Drug Discovery Ministry of Education, School of Pharmaceutical Sciences, Wuhan University, Wuhan 430071, China

Supporting Information

ABSTRACT: Anthrabenzoxocinones (ABXs) including (−)-ABXs and (+)-ABXs are a group of bacterial FabF-specific inhibitors with potent antimicrobial activity of resistant strains. Optimization of their chemical structures is a promising method to develop potent antibiotics. Through biosynthetic investigation, we herein identified and characterized two highly promiscuous enzymes involved in the (−)-ABX structural modification. The promiscuous halogenase and methyltransferase can respectively introduce halogen-modifications into various positions of the ABX scaffolds and methylation to highly diverse substrates. Manipulation of their activity in both of the (−)-ABXs and (+)-ABXs biosyntheses led to the generation of 14 novel ABX analogues of both enantiomers. Bioactivity assessment revealed that a few of the analogues showed significantly improved antimicrobial activity, with the C3-hydroxyl and chlorine substitutions critical for their activity. This study enormously expands the bioactive chemical space of the ABX family and FabF-specific inhibitors. The disclosed broad-selective biosynthetic machineries and structure−activity relationship provide a solid basis for further generation of potent antimicrobial agents.

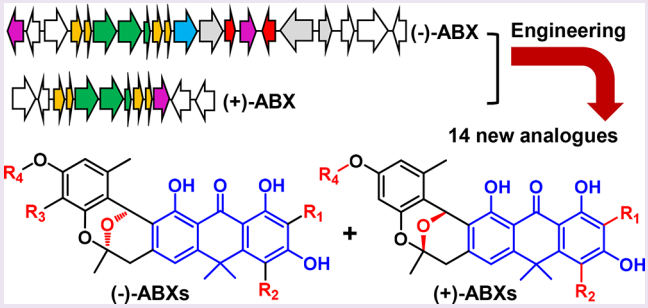

Bacterial infections are one of the greatest health challenges in human beings and animals. With the steady emergence of antibiotic resistance, common infections can once again be lethal. Methicillin-resistant *Staphylococcus aureus* (MRSA) and vancomycin resistant *Enterococcus* (VRE) are two antibiotic resistant strains of bacteria which are now a major concern in hospital settings.[1] Therefore, discovering novel antibiotics with different modes of action is highly desired. Fatty acid synthesis is essential to bacterial cell viability. The significant differences in the structure of fatty acid synthases (FASs) and the role played by fatty acids between bacteria and humans make this system a very attractive target for antibacterial drug discovery.[2]

Anthrabenzoxocinones (ABXs) are a small group of aromatic polyketide compounds with potent antimicrobial activities in addition to other bioactivities.[3−8] Based on the different stereogenic centers at C6 and C16, ABXs can be divided into (−)-ABXs and (+)-ABXs. Currently, six ABX enantiomers, including (−)-ABX-A, (−)-BABX, (+)-ABX-A (also named as BE-24566B, L-755805 and 1.264-C), and (+)-zunyimycin A−C, have been isolated from a few *Streptomyces* strains (Figure 1).[3−8] These molecules possess a pair of unique chiral oxygen-bridged scaffolds and a 1,3-dihydroxy-10,10-dimethylanthrone (DHDA) unit that can bind the condensation enzyme FabF of bacterial FASs with high affinity.[5,9] By utilizing a different protein target from those of methicillin and vancomycin, ABXs are highly active against MRSA and VRE.[4,5,7] Optimization of these scaffolds is a promising avenue to yield antibiotics with increased potencies. Due to the complexity of their chemical structure, optimization through chemical approaches is often challenging, making biosynthetic ways more practicable. For this aim, we herein performed biosynthetic investigation of the (−)-ABX-A and (+)-ABX-A pathways to explore their active chemical space. Through delineation and manipulation of two cryptic broad-selective modification steps, a total of 14 novel analogues of both enantiomers were obtained, resulting in the identification of congeners with significantly increased antimicrobial activities.

RESULTS AND DISCUSSION

Cloning of the ABXs Biosynthetic Gene Clusters. To access the biosynthetic gene clusters of (−)-ABX-A/(−)-BABX and (+)-ABX-A, the genomes of their producer *Streptomyces* sp.

Received: August 25, 2017
Accepted: December 11, 2017
Published: December 11, 2017

DOI: 10.1021/acschembio.7b00743
ACS Chem. Biol. 2018, 13, 200−206

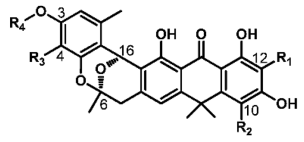

	R_1	R_2	R_3	R_4
(-)-ABX-A	H	H	H	H
(-)-BABX	Cl	Cl	H	CH_3
(-)-ABX-B (**1**)	H	Cl	H	CH_3
(-)-ABX-C (**2**)	Cl	H	H	CH_3
(-)-ABX-D (**3**)	H	Cl	Cl	CH_3
(-)-ABX-E (**4**)	H	H	H	CH_3
(-)-ABX-F (**5**)	Cl	H	H	H
(-)-ABX-G (**6**)	H	Cl	Cl	H
(-)-ABX-H (**7**)	Cl	Cl	H	H
(-)-ABX-I (**8**)	Cl	Cl	Cl	H
(-)-ABX-J (**9**)	Cl	Cl	Cl	CH_3

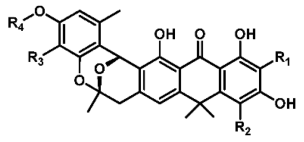

	R_1	R_2	R_3	R_4
(+)-zunyimycin A	H	Cl	Cl	H
(+)-zunyimycin B	Cl	H	Cl	H
(+)-zunyimycin C	Cl	Cl	Cl	H
(+)-ABX-A	H	H	H	H
(+)-ABX-B (**10**)	Cl	H	H	H
(+)-ABX-C (**11**)	H	Cl	H	H
(+)-ABX-D (**12**)	H	H	H	CH_3
(+)-ABX-E (**13**)	Cl	H	H	CH_3
(+)-ABX-F (**14**)	H	Cl	H	CH_3

Figure 1. Structures of previously reported ABXs and the new congeners (**1**−**14**) identified in this study.

MA6657[5] and *Actinomycete* MA7150[3] were sequenced. Analysis of these genomes led to the identification of two homologous loci that encode a type II polyketide synthase (PKS) system (Figure 2A and B, Tables S1 and S2). In the center of these clusters are genes encoding ketosynthase α (KS_α, *abxP*), KS_β (*abxK*), and acyl carrier protein (ACP, *abxS*), which may cooperate with a fatty acid malonyl-CoA transferase[10] to synthesize the linear polyketone substrate. Located close to the

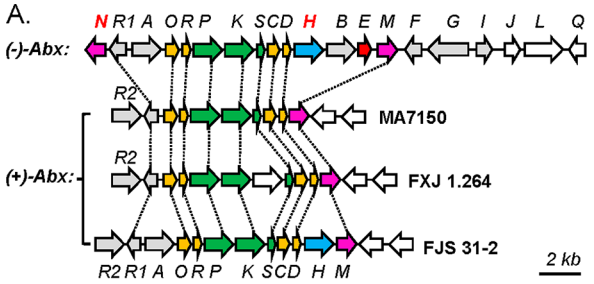

B.

Gene	Function	Gene	Function
J, N, M, Q	Methyltransferase	*K*	KSβ
R1, I	Regulator	*S*	ACP
A-B, G	Transporter	*H*	Halogenase
O	WhiEI-like protein	*E*	Ketoreductase
R, C-D	Aromatase/ cyclase	*F*	Glyoxalase
P	KSα	*L*	Monooxygenase

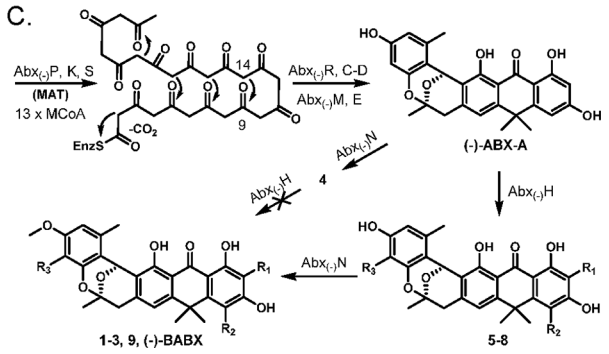

Figure 2. Biosynthetic gene clusters and proposed pathways. (A) Gene organization of the (−)-*abx* and (+)-*abx* clusters. The pivot methyltransferase and halogenase ($abx_{(-)}N$ and *H*) were highlighted in red. (B) Predicted functions of genes (also see Tables S1 and S2). (C) Proposed biosynthesis of (−)-ABXs in the MA6657. R_1−R_3 denote halogen groups.

PKS genes are genes that encode aromatase/cyclase (*abxR, C* and *D*), whiEI-like protein (*abxO*), and methyltransferase (*abxM*) putatively for synthesizing the gem-dimethylated anthracenone scaffold. Interestingly, (+)-ABX pathways including the (+)-*abx* from MA7150 and two recently reported (+)-ABX-A and (+)-zunyimycin pathways from other strains[8] all lack the ketoreductase gene (*abxE*), which is assumed to generate the C16-hydroxyl group for the oxygen-bridged moiety formation. In addition to genes related to scaffold formation, the cluster of MA6657 also contains a halogenase ($abx_{(-)}H$), a flavin-dependent monoxygenase ($abx_{(-)}L$), and three methyltransferases ($abx_{(-)}J$, *N*, and *Q*), as well as several regulators ($abx_{(-)}R1$ and *I*), transporters ($abx_{(-)}A$, *B*, and *G*), and a glyoxalase gene ($abx_{(-)}F$), which are known for conferring the structural modification, gene regulation, and self-immunity.

Characterization of the New ABX Derivatives 1−4 and Promiscuous Halogenation Step. To correlate the (−)-*abx* with (−)-ABX-A/(−)-BABX biosynthesis, the cosmid containing the locus and flanking genes from MA6657 was selected for heterologous expression in the *S. albus* J1074. Analyzing the fermentation broth of the recombinant strain confirmed that both the (−)-ABX-A and (−)-BABX were produced along with four novel products (**1**−**4**; Figure 3, trace I). Isolation and

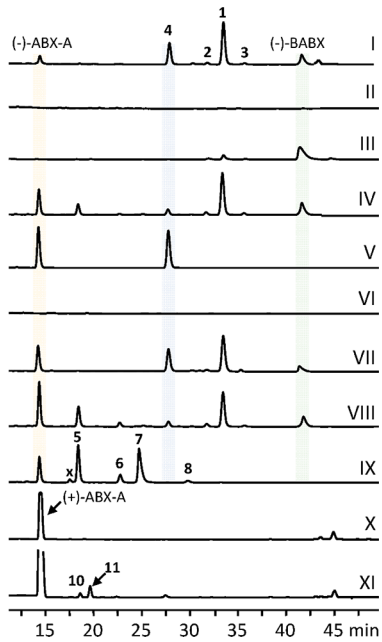

Figure 3. HPLC analysis of (−)-ABXs and (+)-ABXs production in MA6657, FXJ1.264, and *S. albus* J1074 recombinant strains. (I) mWHU2467 (J1074 with 4E10); (II) wild-type J1074; (III) wild-type MA6657; (IV) mWHU2471 ($\Delta abx_{(-)}L$); (V) mWHU2468 ($\Delta abx_{(-)}H$); (VI) mWHU2469 ($\Delta abx_{(-)}M$); (VII) mWHU2470 ($\Delta abx_{(-)}J$); (VIII) mWHU2472 ($\Delta abx_{(-)}Q$); (IX) mWHU2473 ($\Delta abx_{(-)}N$); (X) wild-type FXJ1.264; (XI) mWHU2474 (FXJ1.264 with $abx_{(-)}H$). Compound x, a single chlorinated (−)-ABX-A analogue (based on MS analysis), is not structurally characterized.

structural characterization of **1**−**4** revealed that they are all new congeners, bearing an identical scaffold to the (−)-BABX but different chlorination patterns (Figure 1). Compounds **1** and **2** each have a single chlorine atom at C10 and C12, respectively. Compound **3** has two chlorines with one at a novel position (C4), and **4** is nonchlorinated. The various chlorination

DOI: 10.1021/acschembio.7b00743
ACS Chem. Biol. 2018, 13, 200−206

patterns suggest the corresponding halogenase has a very broad selectivity. To identify the enzyme involved, we individually deleted the two FAD-dependent oxidoreductase genes ($abx_{(-)}H$ and $abx_{(-)}L$), which are theoretically able to catalyze the chlorination reaction. Deletion of $abx_{(-)}L$ shows no influence on **1**−**3** and (−)-BABX biosynthesis while $abx_{(-)}H$ inactivation completely abolished their production (Figure 3, trace IV and V). Thus, $abx_{(-)}H$ is indeed responsible for the chlorination modification. In order to characterize the halogenation activity in detail, $abx_{(-)}H$ was overexpressed in *Escherichia coli*, and the enzyme was purified and biochemically assayed. In the presence of NaCl, flavin reductase, and NADPH, $Abx_{(-)}H$ is able to convert the (−)-ABX-A into five novel products (Figure 4, trace II) whose molecular weights

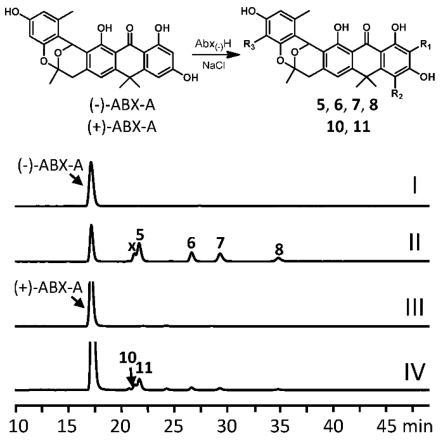

Figure 4. Characterization of the chlorination activity of $Abx_{(-)}H$. (I) Standard (−)-ABX-A. (II) $Abx_{(-)}H$ reaction, converting (−)-ABX into **5**−**8**. The peak indicated by x is same to the x in the Figure 3. (III) Standard (+)-ABX-A. (IV) $Abx_{(-)}H$ reaction, converting (+)-ABX-A into **10** and **11**.

correspond to monochlorinated, dichlorinated, and trichlorinated analogues, respectively (**5**−**8**, structural characterization see below). Switching the NaCl to NaBr resulted in two monobrominated products (Figure S1, trace II). Moreover, $Abx_{(-)}H$ can also catalyze bromination on the chlorinated substrate **5** to generate two chlorine-bromine hybrid products (Figure S1, trace IV). These results together successfully identified a highly broad-selective halogenase, which is able to generate the diverse structural variety of ABXs.

Characterization of the Promiscuous Methylation Step and Novel ABX Derivatives 5−**9.** The identical C3-hydroxylmethyl group in **1**−**4** and (−)-BABX indicates there exists another broad-selective modification. (−)-*abx* contains four methyltranferase genes ($abx_{(-)}M$, *N*, *J*, and *Q*), whose function fit this role. To confirm their involvement, these four genes were individually deleted from the cluster. Analysis of the fermentation broth revealed that (i) $abx_{(-)}M$ is necessary for the scaffold formation (Figure 3, trace VI), which is consistent with the assumption of conferring the gem-dimethylation of the anthracenone scaffold; (ii) $abx_{(-)}N$ is essential for production of **1**−**4** and (−)-BABX; and (iii) $abx_{(-)}J$ and *Q* are not related to the (−)-ABXs biosynthesis (Figure 3, trace IX, VII, and VIII). Deletion of $abx_{(-)}N$ can produce five novel products whose retention times and molecular weights are the same as those in the $Abx_{(-)}H$ reaction (Figure 4, trace II). By scaling up the fermentation, four major products (**5**−**8**) were further isolated and characterized (Figure 1). These new products are all nonmethylated chlorinated products, among which **5** bears a single chlorine at C12, **6** and **7** are dichlorinated at C4−C10 and C10−C12, respectively, and **8** is trichlorinated at C4, C10, and C12. On the basis of their fermentation titer, it is revealed that the most favorable chlorination route for $Abx_{(-)}H$ is from C12 and C12−C10 to C12−C10−C4. Interestingly, in the wild-type strain, $Abx_{(-)}H$ cannot convert the C3−OH methylated product (data not shown). This can lead to some unfavorable chlorinated products, such as C10 monochlorination, accumulating as the major methylated products (*e.g.*, **1**, Figure 3, trace I). While favorable, monochlorinated intermediates (*e.g.*, **2**, Figure 3, trace I) are produced in low yield due to rapid conversion into multichlorinated products before methylation. This antagonistic relationship between $Abx_{(-)}N$ and H make this pathway very effective for generating structural varieties. To characterize the methylation activity in detail, $Abx_{(-)}N$ was further overexpressed. A biochemical assay revealed that $Abx_{(-)}N$ is able to convert all of the isolated nonmethylated substrates (**5**−**8** and (−)-ABX-A) into the corresponding methylated products (**2**−**4**, **9** and (−)-BABX; Figure 5 and Figure S2). Interestingly, **9** is not produced by the

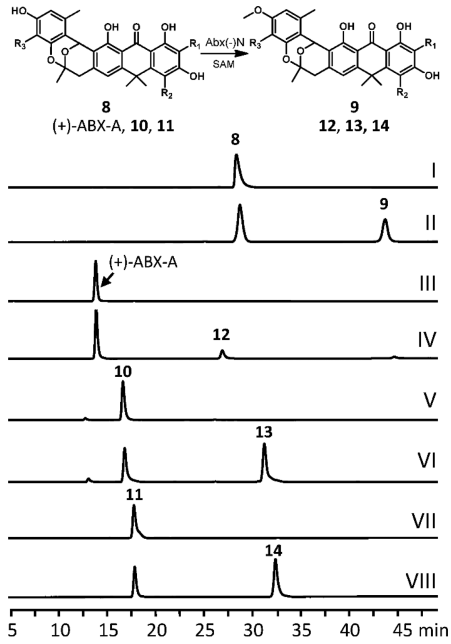

Figure 5. Characterization of the methylation activity of $Abx_{(-)}N$. (I) Standard **8**. (II) $Abx_{(-)}N$ reaction, converting **8** into **9**. (III) Standard (+)-ABX-A. (IV) $Abx_{(-)}N$ reaction, converting (+)-ABX-A into **12**. (V) Standard **10**. (VI) $Abx_{(-)}N$ reaction, converting **10** into **13**. (VII) Standard **11**. (VIII) $Abx_{(-)}N$ reaction, converting **11** into **14**.

heterologous expression strain mWHU2467 (Figure 3, trace I). Through a preparative-scale enzymatic transformation, it was isolated in sufficient quantity for confirmation by NMR analysis. Taken together, these results successfully identified a second broad-selective modification in (−)-ABX biosynthesis. Manipulating its activity provides an effective way to generate diverse analogues.

Engineering (+)-*abx* with the Promiscuous Methyltransferase and Halogenase to Generate Novel ABX Analogues 10−**14.** Since (−)-ABXs and (+)-ABXs have an identical FabF-binding DHDA unit, both of these molecules have potent antimicrobial activity.[3−8] Compared to the (−)-ABXs, (+)-ABXs are structurally less diverse, and only

DOI: 10.1021/acschembio.7b00743
ACS Chem. Biol. 2018, 13, 200−206

four members have been identified so far. Considering $Abx_{(-)}H$ and $Abx_{(-)}N$ have broad selectivity, we are interested in utilizing these biosynthetic machineries to modify the scaffold of (+)-ABX. We confirmed by *in vitro* assay that both the $Abx_{(-)}H$ and N enzymes are able to individually convert the (+)-ABX-A substrate into two monochlorinated and one methylated products (Figure 4, trace IV and Figure 5). By scaling up the reaction, the methylated product was isolated and confirmed as the C3-hydroxyl methylated (+)-ABX (**12**; Figure 1). This is interesting because the benzyl substructures in (−)-ABX-A and (+)-ABX-A are bent to an opposite direction. The efficient methylation of C3-OH by $Abx_{(-)}N$ suggests it has a flexible binding cavity to accommodate highly different molecules, which could be useful for engineering other scaffolds. In order to isolate the chlorinated products, $abx_{(-)}H$ was introduced into FXJ1.264. The metabolite profile in its fermentation broth is identical to the enzymatic reaction, and two of the major products (**11** and **10**; Figure 1) were isolated and confirmed as C10 and C12 monochlorinated (+)-ABX-A, respectively. In addition, by incubating **10** and **11** with $Abx_{(-)}N$, these products were further converted into two novel C3-hydroxylmethylated products **13** and **14**, respectively (Figure 5, trace VI and VIII). The successful engineering of (+)-ABX indicates that both $Abx_{(-)}N$ and H are highly tolerant to structural variation, which can potentially be used to engineer many other DHDA-containing products.[11−14] Similarly, promiscuous halogenase in the other DHDA-containing product[11] may also be suitable to engineer ABXs. Halogen atoms are very useful handles in chemical synthesis, which can be readily converted into other groups through coupling reactions. $Abx_{(-)}H$ can directly modify small molecules and does not require the ACP for activity. Its broad selectivity provides an effective tool to introduce diverse substitutions into the DHDA-containing molecules that will benefit the development of novel antibiotics.

Activity Assay of the New ABXs. Finally, all of generated products (**1**−**14**), except **13**, due to inadequate quantity, were assessed for antimicrobial activity. Similar to other ABXs, these compounds show no obvious effect (MIC > 100 μg mL^{-1}) on the Gram-negative *E. coli* ATCC 25922 or the fungus *Candida albicans* ATCC 10231 (data not shown). However, for Gram-positive strains, most of the compounds show improved antimicrobial activity compared to (−)-ABX-A, (−)-BABX, (+)-ABX-A, and (+)-zunyimycin A−C.[7] Among them, **6** and **8** show the best activity against *Staphylococcus aureus* ATCC 51650 and *Bacillus subtilis* ATCC 23857 and are 7.0- and 3.5-fold more potent than the previous best products (+)-ABX-A and (−)-BABX, respectively (Table 1). Comparing the molecules to their corresponding C3-methylated congeners, including the pairs of **6**/**3**, **8**/**9**, **12**/(+)-ABX-A, and **11**/**14**, it can be concluded that the C3-hydroxyl group is crucial for both (−)- and (+)-ABX activity. More so, chlorines are beneficial for both of the (−) and (+)-ABX activity, and the variation of their substitution position and numbers can alter the selection of antimicrobial activity between *B. subtilis* and *S. aureus*. For instance, multiple chlorinations increase the potency to *B. subtilis*, while di- or mono-chlorination in the C10 and C12 are best against *S. aureus*. These results together identified congeners with significantly improved antimicrobial activity and show a clear way for further engineering the active scaffold of the FabF inhibitor.

Table 1. MIC (μg mL^{-1}) Data for 1−12 and 14 against *Bacillus subtilis* ATCC 23857 (*B. S*) and *S. aureus* ATCC 51650 (*S. A*)

comp.	*B. S*	*S. A*	comp.	*B. S*	*S. A*
(−)-ABX-A	4.94	3.71	**6**	0.82	0.22
(−)-BABX	1.57	1.59	**7**	0.51	0.88
(+)-ABX-A	1.76	1.54	**8**	0.45	0.91
1	0.47	0.61	**9**	2.80	5.21
2	0.89	1.94	**10**	1.19	1.02
3	22.65	10.06	**11**	0.9	0.90
4	2.86	3.31	**12**	2.86	14.70
5	0.88	0.32	**14**	5.77	6.13

CONCLUSIONS

In summary, we have identified two biosynthetic pathways of a pair of ABX enantiomers. Based on *in vitro* and *in vivo* characterization, two broad-selective methylation and chlorination steps were deciphered. Manipulation of their activity in both of the (−)-ABX and (+)-ABX biosynthetic pathways has led to the production of 14 novel chlorinated/methylated products, which includes compounds with significantly improved antimicrobial activity. Assessment of their activity revealed that both of the C3-hydroxyl and chlorine substitutions (numbers and positions) are critical for antimicrobial activity. This study has significantly expanded the bioactive chemical space of the ABX family and FabF-specific inhibitors. The revealed biosynthetic machineries and structure−activity relationship lays a solid stage for further generation of potent antimicrobial agents.

METHODS

General Materials and Methods. *Escherichia coli* and *Streptomyces* strains were cultivated and manipulated according to the standard methods.[15,16] Strains, plasmids, and primers used in this study are listed in Tables S3 and S4, respectively. *Actinomycete* MA7150, *Streptomyces* sp. FXJ1.264, *Streptomyces* sp. MA6657, and *Streptomyces albus* J1074 wild-type and recombinant strains were cultivated either on the medium mannitol soy flour (MS) agar for sporulation or on tryptic soy broth (TSB) for growth. DNA isolation and gene manipulation in *E. coli* were carried out using standard methods.[15] Genome sequencing of MA7150 and MA6657 were performed by Shanghai Hanyu Bio-Tech Co. Ltd. using the HiSeq 2500 System. Primer synthesis and DNA sequencing were performed at Genewiz Biotech Co., Ltd. (China). Restriction enzymes and DNA polymerases (Taq and PrimeSTAR) were purchased from Takara Biotechnology Co., Ltd. (China). All chemicals and reagents were purchased from Santa Cruz Biotechnology, Inc. (USA) or Shanghai Sangon Biotech (China) Co., Ltd. unless noted otherwise.

Genomic Library Construction and Screening. The genomic library of MA6657 was constructed into the cosmid pJTU2554, which contains *oriT*, *φC31-int*, and *attp* for conjugation and integration into a *Streptomyces* host. Briefly, genomic DNA of MA6657 was digested into fragments of around 42 kb in size by *Sau*3AI, dephosporylated by SAP (shrimp alkalinephosphatase), and recovered. Cosmid pJTU2554 was digested by *Hpa*I, dephosporylated by SAP, and then digested by *Bam*HI to generate two 7.5 kb and 2 kb vector fragments. The prepared DNA fragments were subsequently ligated with the treated pJTU2554 vector fragments and then packaged by MaxPlaxTM Lambda PackagingExtracts (Illumina, Inc. USA) before transfection into *E. coli* EPI300 TM-T1. The resulting *E. coli* clones were harvested and stored at −80 °C. The Cosmid 4E10 containing the ABX gene cluster were acquired by PCR screening and determined by termini sequencing.

Heterologous Expression in *S. albus* J1074. The wild-type recombinant strain mWHU2467 was acquired by conjugation of

DOI: 10.1021/acschembio.7b00743
ACS Chem. Biol. 2018, 13, 200−206

cosmid 4E10 into *S. albus* J1074 following the standard method described before.[17] Gene-deleted recombinant strains were prepared as follows. Briefly, for $abx_{(-)}N$, *L* and *Q* deletion, the selectable marker *bla* from the plasmid pSP72 was amplified by the primer pairs abxN-amp-F/R, abxL-amp-F/R, and abxQ-amp-F/R and then electro-transformed into the *E. coli* GB05 competent cells containing the cosmid 4E10 to induce gene replacement. For $abx_{(-)}H$, $abx_{(-)}M$, and $abx_{(-)}J$ deletion, the *aada* from the plasmid pIJ778 was first amplified by primer pair pSP-pIJ778-F/R. The resulting *aada* fragment was further served as a template for PCR to add terminal recombination arms by primer pairs abxH-aada-F/R, abxM-aada-F/R, and abxJ-aada-F/R. These fragments were then electro-transformed into the *E. coli* GB05 competent cells containing the cosmid 4E10 to induce gene replacement. Colonies grew on the apramycin and spectinomycin ($abx_{(-)}H$, *M* and *J*) or ampicillin ($abx_{(-)}N$, *L*, and *Q*) were selected for cosmid isolation. After confirmation by restriction analysis and PCR, cosmids were digested by *Nde*I and self-ligated by T4 ligase to remove the internal resistant markers. The resulting constructs pWHU2462-pWHU2467 corresponding to $abx_{(-)}H$, *M*, *J*, *L*, *Q*, and *N* deletion were further introduced into the *E. coli* ET12567/pUZ8002 and then to *S. albus* J1074 *via* conjugation with MS as a medium according to standard protocol. Colonies with apramycin resistance were selected and confirmed by PCR to yield the recombinant strains mWHU2468 mWHU2473.

Complement $abx_{(-)}H$ into *S. sp.* FXJ1.264. AbxH was amplified from the genomic DNA of MA6657 by primer pair abxH-ht-F/R. This DNA fragment was further digested by *Nde*I-*Eco*RI and cloned into the same sites of pIB139. After being proofed by DNA sequencing, the generated plasmid pWHU2468 was introduced into the FXJ1.264 *via* conjugation to generate the recombinant strain mWHU2474 through an identical procedure to that above.

Cloning, Overexpression, and Purification of Recombinant Proteins. Genes of $Abx_{(-)}H$ and $Abx_{(-)}N$ were amplified by primer pairs AbxH-F/R and AbxN-F/R, respectively, from 4E10. The *Nde*I-*Hin*dIII fragments were cloned into pET28a to generate expression plasmids pWHU2469 and pWHU2470. After being proofed by DNA sequencing, these plasmids were then transformed into *E. coli* BL21 (DE_3) for overexpression of N-terminal 6 × His-tagged fusion proteins. In 0.5 L of liquid culture, the cells were grown at 37 °C in LB medium with 50 $\mu g\ mL^{-1}$ kanamycin to an OD_{600} of 0.5−0.8. The cells were cooled to 16 °C and then induced by 0.1 mM isopropyl-β-D-thiogalactopyranoside (IPTG) for 24 h. The cells were harvested by centrifugation, resuspended in 30 mL of lysis buffer (25 mM HEPES, pH 7.5, 300 mM NaCl, 5 mM imidazole, 10% (v/v) glycerol), and lysed by sonication. After centrifugation (15 000 rpm, 30 min, 4 °C), Ni-NTA agarose resin was added to the supernatant (2 mL L^{-1} of culture), and the solutions were shaken at 4 °C for 30 min. The protein resin mixtures were loaded into a gravity flow column, and proteins were eluted with increasing concentrations of imidazole (25 mM, 50 mM, 100 mM, 300 mM) in Buffer A (25 mM HEPES, pH 7.5, 300 mM NaCl, 10% (v/v) glycerol). Proteins were further concentrated by centrifugation using an Amicon Ultra-4 (10 kDa, GE Healthcare). Proteins' purities were evaluated by 10% (w/v) acrylamide SDS-PAGE, and concentrations were determined by the Bradford method using a BSA calibration curve.

In vitro Enzymatic Assay of $Abx_{(-)}H$. Typical assays were performed in 400 μL of 100 mM PBS buffer (100 mM potassium phosphate, pH 6.0) containing 27 μM substrates including (−)-ABX-A, (+)-ABX-A and their analogues, 50 mM NaCl (or NaBr), 0.125 mM FDA, 25 μM Fre, 50 mM glucose, 23.5 μM glucose dehydrogenase (GDH), 10 mM NADH, and 26 μM $Abx_{(-)}H$. Reactions were incubated at 30 °C for 4 h, quenched by 3 volumes of ethyl acetate. The organic phases were evaporated by vacuum, and the resulting residues were redissolved by 100 μL of methanol, which was further subjected to HPLC or LC-HRMS analysis using an analytic Inertsil ODS-3 column (5 μm, 4.6 × 250 mm, GL Science Inc.). HPLC analysis was normally performed at a flow rate of 1 mL/min and a UV detection at 360 nm over a 50 min gradient program: *T* = 0 min, 60% B; *T* = 45 min, 95% B; *T* = 46 min, 95% B; *T* = 47 min, 60% B; *T* = 50 min, 60% B (A = H_2O, B = CH_3CN + 0.1% HCO_2H). For HPLC-ESI-MS analysis, conditions are the same as for the HPLC analysis.

***In Vitro* Enzymatic Assay of $Abx_{(-)}N$.** Typical assays were performed in 400 μL of 100 mM PBS buffer (100 mM potassium phosphate, pH 8.0) containing 25 μM substrates including (−)-ABX-A, (+)-ABX-A and their analogues, 5 mM SAM, 5 mM $MgCl_2$, and 27 μM enzyme. Reactions were incubated at 28 °C overnight, quenched by three volumes of ethyl acetate. The organic phase was evaporated by vacuum, and the resulting residues were redissolved by 100 μL of methanol, which were further subjected to HPLC or LC-HRMS analysis using an identical analytic column and separation condition to that above.

Production, Isolation and Purification of ABX Analogues. *Compounds **1**−**4**, (−)-ABX-A, and (−)-BABX.* For large-scale production, the freshly prepared spores of mWHU2467 (grew on MS media) were inoculated into the MA6657 production medium (30 × 300 mL), and the cultures were grown at 30 °C and 220 rpm for 7 days. The broth was extracted with an equal volume of ethyl acetate three times. The organic phase was combined and further removed by rotary evaporation. The crude extract (3.0 g) was subjected to CC on silica gel and was eluted with a gradient of petroleum ether/ethyl acetate from 100:0 to 0:100 (v/v) to give six fractions (fraction 1−6) on the basis of TLC analysis. Fraction 2 was subjected to a Sephadex LH-20 eluted with CH_2Cl_2/MeOH (1:1) to obtain subfractions 1A−1C, and the subfraction 1B was further purified by HPLC (MeCN/H_2O, 90:10, 1.8 mL/min) to afford **1** (38.0 mg), **3** (2.0 mg), and (−)-BABX (12.8 mg). Fraction 3 was separated using the same method as described above to yield **4** (11.6 mg) and **2** (2.9 mg). Fraction 4 was also separated using the same method to afford (−)-ABX-A (8.1 mg).

*Compounds **5**−**8**.* Similar to the above condition, the freshly prepared spores of mWHU2473 (grew on MS media) were inoculated into the MA6657 production medium (30 × 300 mL), and the cultures were grown at 30 °C and 220 rpm for 7 days. The broth was extracted with an equal volume of ethyl acetate three times. The organic phase was combined and further removed by rotary evaporation. The crude extract (8.44 g) was subjected to CC on silica gel and was eluted with a gradient of petroleum ether/ethyl acetate from 100:0 to 0:100 (v/v) to give five fractions (fraction 1−5) on the basis of TLC analysis. Fraction 3 was separated by HPLC with a linear gradient of 75−95% MeCN/H_2O over 32 min at a flow rate of 2 mL min^{-1} to afford **5** (5.3 mg), **8** (5.7 mg), and a mixture of **6** and **7**. The mixture of **6** and **7** was then separated by HPLC (MeCN/H_2O, 80:10, 2 mL min^{-1}) to give **6** (3.7 mg) and **7** (5.6 mg).

*Compound **9**.* Compound **9** was produced by enzymatic assays and further purified by HPLC to obtain **9** (1.2 mg).

*Compounds **10**−**11**, (+)-ABX-A.* For large-scale production, the mWHU2474 TSB culture broth was inoculated onto the GYM medium (100 × 80 mL) and grew at 30 °C for 7 days. The culture medium was cut into small pieces and extracted with an equal volume of ethyl acetate three times. The extracting solution was filtered and evaporated to remove ethyl acetate. The crude extract (8.44 g) was subjected to CC on silica gel and was eluted with a gradient of petroleum ether/ethyl acetate from 100:0 to 0:100 (v/v) to give 12 fractions (fractions 1−12) on the basis of TLC analysis. Fraction 9 was separated by HPLC (MeCN/H_2O, 90:10, 1.8 mL/min) to afford **11** (12.3 mg). Fraction 10 was subjected to a Sephadex LH-20 eluted with CH_2Cl_2/ MeOH (1:1) to obtain subfractions 1A−1G, and the subfraction 1F was further purified by HPLC (MeCN/H_2O, 75:20, 1.8 mL/min) to afford (+)-ABX-A (40.0 mg) and **10** (2.7 mg).

*Compounds **12** and **14**.* These three compounds were also produced by enzymatic assays, further purified by HPLC (see above) to obtain **12** (0.9 mg) and **14** (0.8 mg).

Structural Elucidation of the Isolated Compounds. *(−)-ABX-A.* Yellow amorphous powder. $[\alpha]_D^{20}$ −132.0° (*c* 0.05 MeOH). ESI-HRMS *m*/*z* 461.1568 $[M + H]^+$ (calcd for 461.1600, $C_{27}H_{24}O_7$). ^1H NMR (400 MHz, CD_3OD) and ^{13}C NMR (100 MHz, CD_3OD), see Table S5 and attached spectra Supplementary Figures S3 and S4. Comparing ^1H NMR and ^{13}C NMR to the reference[5] showed it was (−)-ABX-A.

DOI: 10.1021/acschembio.7b00743
ACS Chem. Biol. 2018, 13, 200−206

(−)-BABX. Yellow amorphous powder. $[\alpha]_D^{20}$ −121.54° (*c* 0.26 MeOH). ESI-HRMS *m/z* 543.0948 $[M + H]^+$ (calcd for 543.0977, $C_{28}H_{24}O_7Cl_2$). ^1H NMR (400 MHz, CD_3OD) and ^{13}C NMR (100 MHz, CD_3OD), see Table S6 and attached spectra Supplementary Figures S5 and S6. Comparing ^1H NMR and ^{13}C NMR to the reference[5] showed it was (−)-BABX.

Compound 1 ((−)-ABX-B). Yellow amorphous powder. $[\alpha]_D^{20}$ −269.4° (*c* 0.55 MeOH). Mass spectral analysis of compound **1** provided a molecular formula of $C_{28}H_{25}O_7Cl$. ESI-HRMS *m/z* 509.1338 $[M + H]^+$ (calcd for 509.1367), which was supported by ^{13}C NMR (see Table S6 and Figure S8). The comparison of ^1H NMR (see Table S6 and Figure S7) spectra of **1** and (−)-ABX-A indicated the presence of a methoxy group (δ_H 3.71) and the absence of H-10, which were replaced by a chlorine atoms in compound **1**. The methoxy protons afforded an HMBC (Figure S10) correlation to C-3 (δ_C 159.4), confirming the location of methoxy at C-3. As expected, C8, C12, C13a, and C14 did not show HMBC correlations, indicating the location of chlorine atoms at C-10. On the basis of these data, structure **1** was assigned to (−)-ABX-B.

Compound 2 ((−)-ABX-C). Yellow amorphous powder. $[\alpha]_D^{20}$ −262.5° (*c* 0.12 MeOH). Mass spectral analysis of compound **2** provided a molecular formula of $C_{28}H_{25}O_7Cl$. ESI-HRMS *m/z* 509.1338 $[M + H]^+$ (calcd for 509.1367), which was supported by ^{13}C NMR (see Table S5 and Figure S12). The ^1H NMR (see Table S5 and Figure S11) spectra of **2** were exactly that same as those of **1**. However, C8, C12, C13a, and C14 show HMBC (Figure S14) correlations with H-10 (δ_H 6.80), indicating the location of chlorine atoms at C-12. On the basis of these data, structure **2** was assigned to (−)-ABX-C.

Compound 3 ((−)-ABX-D). Yellow amorphous powder. $[\alpha]_D^{20}$ −25.6° (*c* 0.16 MeOH). Mass spectral analysis of compound **3** provided a molecular formula of $C_{28}H_{24}O_7Cl_2$. ESI-HRMS *m/z* 543.0948 $[M + H]^+$ (calcd for 543.0977), which was supported by ^{13}C NMR (see Table S6 and Figure S16). The ^1H NMR (see Table S6 and Figure S15) spectra of **3** were exactly the same as those of (−)-BABX. However, the linkages of C-10 and C-13a were determined by the HMBC correlations of H-12; C4 and C16a did not show HMBC (Figure S18) correlations, indicating the location of chlorine atoms at C-12 and C-4. On the basis of these data, structure **3** was assigned to (−)-ABX-D.

Compound 4 ((−)-ABX-E). Yellow amorphous powder. $[\alpha]_D^{20}$ −444.3° (*c* 1.0 CH_2Cl_2). Mass spectral analysis of compound **4** provided a molecular formula of $C_{28}H_{26}O_7$. ESI-HRMS *m/z* 475.1724 $[M + H]^+$ (calcd for 475.1757), which was supported by ^{13}C NMR (see Table S5 and Figure S20). The comparison of ^1H NMR (see Table S5 and Figure S19) spectra of **4** and (−)-ABX-A indicated the presence of a methoxy group (δ_H 3.65). The methoxy protons afforded an HMBC (Figure S22) correlation to C-3 (δ_C 159.3), confirming the location of methoxy at C-3. On the basis of these data, structure **4** was assigned to (−)-ABX-E.

Compound 5 ((−)-ABX-F). Yellow amorphous powder. $[\alpha]_D^{20}$ −154.17° (*c* 0.12 MeOH). Mass spectral analysis of compound **5** provided a molecular formula of $C_{27}H_{23}O_7Cl$. ESI-HRMS *m/z* 495.1181 $[M + H]^+$ (calcd for 495.1211). The comparison of ^1H NMR (see Table S7 and Figure S23) spectra of **5** and **2** indicated the absence of a methoxy group at C-3 and slightly changed the chemical shift of H-2 and H-4. On the basis of these data, structure **5** was assigned to (−)-ABX-F.

Compound 6 ((−)-ABX-G). Yellow amorphous powder. Mass spectral analysis of compound **6** provided a molecular formula of $C_{27}H_{22}O_7Cl_2$. ESI-HRMS *m/z* 529.0803 $[M + H]^+$ (calcd for 529.0821), which was supported by ^{13}C NMR (see Table S7 and Figure S25). The comparison of ^1H NMR (see Table S7 and Figure S24) spectra of **6** and **3** indicated the absence of a methoxy group at C-3. On the basis of these data, structure **6** was assigned to (−)-ABX-G.

Compound 7 ((−)-ABX-H). Yellow amorphous powder. $[\alpha]_D^{20}$ −197.8° (*c* 0.5 MeOH). Mass spectral analysis of compound **7** provided a molecular formula of $C_{27}H_{22}O_7Cl_2$. ESI-HRMS *m/z* 529.0798 $[M + H]^+$ (calcd for 529.0821). The comparison of ^1H NMR (see Table S7 and Figure S28) spectra of **7** and (−)-BABX indicated the absence of a methoxy group at C-3. On the basis of these data structure, **7** was assigned to (−)-ABX-H.

Compound 8 ((−)-ABX-I). Yellow amorphous powder. $[\alpha]_D^{20}$ −362.5° (*c* 0.32 CH_2Cl_2). Mass spectral analysis of compound **8** provided a molecular formula of $C_{27}H_{21}O_7Cl_3$. ESI-HRMS *m/z* 563.0412 $[M + H]^+$ (calcd for 563.0431), which was supported by ^{13}C NMR (see Table S7 and Figure S30). The comparison of ^1H NMR (see Table S7 and Figure S29) spectra of **8** and (−)-ABX-A indicated the absence of three hydrogen atoms, which were replaced by three chlorine atoms in compound **8**. The H-2 (δ_H 6.33) afforded an HMBC (Figure S32) correlation to C-3 (δ_C 152.9), C-17 (δ_C 17.9), and C-16a (δ_C 115.5), confirming the location of chlorine atoms at C-4, C-10, and C-12. On the basis of these data, structure **8** was assigned to (−)-ABX-I.

Compound 9 ((−)-ABX-J). Yellow amorphous powder. Mass spectral analysis of compound **8** provided a molecular formula of $C_{28}H_{23}O_7Cl_3$. ESI-HRMS *m/z* 579.0551 $[M + H]^+$ (calcd for 576.0509). The comparison of ^1H NMR (see Table S8 and Figure S33) spectra of **9** and **8** indicated the presence of a methoxy group (δ_H 3.83). On the basis of these data structure **9** was assigned to (−)-ABX-J.

(+)-ABX-A. Yellow amorphous powder. $[\alpha]_D^{20}$ +125.4° (*c* 0.7 MeOH); ESI-HRMS *m/z* 461.1568 $[M + H]^+$ (calcd for 461.1600, $C_{27}H_{24}O_7$). ^1H NMR (400 MHz, d_6-DMSO) and ^{13}C NMR (100 MHz, d_6-DMSO), see Supporting Table S8 and attached spectra Supporting Figures S34 and S35. Comparing ^1H NMR and ^{13}C NMR to the reference[6] showed it was (+)-ABX.

Compound 10 ((+)-ABX-B). Yellow amorphous powder. Mass spectral analysis of compound **10** provided a molecular formula of $C_{27}H_{23}O_7Cl$. ESI-HRMS *m/z* 495.1181 $[M + H]^+$ (calcd for 495.1211). The comparison of ^1H NMR (see Table S8 and Figure S36) spectra of **10** and **5** indicated structure **10** was assigned to (+)-ABX-B.

Compound 11 ((+)-ABX-C). Yellow amorphous powder. $[\alpha]_D^{20}$ +221° (*c* 0.1 MeOH). Mass spectral analysis of compound **11** provided a molecular formula of $C_{27}H_{23}O_7Cl$. ESI-HRMS *m/z* 495.1181 $[M + H]^+$ (calcd for 495.1211). The comparison of ^1H NMR (see Table S8 and Figure S37) spectra of **11** and (+)-ABX showed the absence of hydrogen atoms which were replaced by a chlorine atoms then compared with **1** showed the absence of a methoxy group at C-3 and slightly changed of the chemical shift of H-2 and H-4. On the basis of these data structure **11** was assigned to (+)-ABX-C.

Compound 12 ((+)-ABX-D). Yellow amorphous powder. Mass spectral analysis of compound **12** provided a molecular formula of $C_{28}H_{26}O_7$. ESI-HRMS *m/z* 475.1724 $[M + H]^+$ (calcd for 475.1757). The ^1H NMR (see Table S8 and Figure S39) spectra indicate compound **12** was similar to compound **4**. On the basis of these data, structure **12** was assigned to (+)-ABX-D.

Compound 13 ((+)-ABX-E). The identity of compound **13** ((+)-ABX-E) was confirmed by comparing with the retention time and molecular weight of **2** through HPLC and MS analysis. **13** has the same retention time as **2** in HPLC and a molecular weight (*m/z* $[M + H]^+$ 509.1346) to its molecular formula of $C_{28}H_{26}ClO_7^+$ (calcd for 509.1367). These data can confirm **13** has an identical planar structure to **2**. Because **13** is the methylated product of (+)-ABX-A, the stereoconfiguration should be the same as (+)-ABX-A. On the basis of these results, the identity of **13** can be finally confirmed, which is illustrated in Figure S40.

Compound 14 ((+)-ABX-F). Yellow amorphous powder. Mass spectral analysis of compound **1** provided a molecular formula of $C_{28}H_{25}O_7Cl$. ESI-HRMS *m/z* 509.1338 $[M + H]^+$ (calcd for 509.1367). The ^1H NMR (see Table S8 and Figure S41) spectra indicate compound **14** was similar to compound **1**. On the basis of these data. structure **14** was assigned to (+)-ABX-F.

Antimicrobial Activity Assay. *E. coli* ATCC 25922, *Staphylococcus aureus* ATCC 51650, *Candida albicans* ATCC 10231, and *Bacillus subtilis* ATCC 23857 were used for MIC determination. MICs were determined by the broth microdilution method. Recommended

DOI: 10.1021/acschembio.7b00743
ACS Chem. Biol. 2018, 13, 200−206

cells used were taken from an overnight culture in fresh LB at 37 °C. These assays were carried out in a 15 mL bottle containing 3 mL of LB with compounds ranged from 0.1 μg mL^{-1} to 25 μg mL^{-1}. Cells were inoculated with a final concentration corresponding to an OD_{600} of 0.08−0.15. The MIC data were achieved at the point where there is no observable growth after overnight incubation.

■ ASSOCIATED CONTENT

Supporting Information

The Supporting Information is available free of charge on the ACS Publications website at DOI: 10.1021/acschembio.7b00743.

Supporting tables, including information on *orfs*, bacteria strains, primers, and NMR data; supporting figures, including biochemical characterization data and NMR spectra (PDF)

■ AUTHOR INFORMATION

Corresponding Authors

*E-mail: chunlei@fudan.edu.cn.
*E-mail: quxd@whu.edu.cn.

ORCID

Xudong Qu: 0000-0002-3301-8536

Author Contributions

‖These authors contributed equally.

Notes

The authors declare no competing financial interest.

■ ACKNOWLEDGMENTS

We thank S. Singh from Merck Co. Ltd.; Y. Huang from Institute of Microbiology CAS for gifting the strains MA6657, MA7150 (Merck), and FXJ 1.264 (IM), respectively. This work was supported by the NSFC (31270119 and 31322002).

■ REFERENCES

(1) Laxminarayan, R., Duse, A., Wattal, C., Zaidi, A. K. M., Wertheim, H. F. L., Sumpradit, N., Vlieghe, E., Hara, G. L., Gould, I. M., Goossens, H., Greko, C., So, A. D., Bigdeli, M., Tomson, G., Woodhouse, W., Ombaka, E., Peralta, A. Q., Qamar, F. N., Mir, F., Kariuki, S., Bhutta, Z. A., Coates, A., Bergstrom, R., Wright, G. D., Brown, E. D., and Cars, O. (2013) Antibiotic resistance-the need for global solutions. *Lancet Infect. Dis. 13*, 1057−1098.

(2) Wang, Y., and Ma, S. (2013) Recent advances in inhibitors of bacterial fatty acid synthesis typeII (FASII) system enzymes as potential antibacterial agents. *ChemMedChem 8*, 1589−1608.

(3) Lam, Y. K. T., Hensens, O., Helms, G., Williams, D., Nallin, M., Smith, J., Gartner, S., Rodriguez, L. H., and Stevens-Miles, S. (1995) L-755,805, a new polyketide endothelin binding inhibitor from an Actinomycete. *Tetrahedron Lett. 36*, 2013−2016.

(4) Kojiri, K., Nakajima, S., Fuse, A., Suzuki, H., and Suda, H. (1995) BE-24566B, a new antibiotic produced by Streptomyces violaceus-niger. *J. Antibiot. 48*, 1506−1508.

(5) Herath, K. B., Jayasuriya, H., Guan, Z., Schulman, M., Ruby, C., Sharma, N., MacNaul, K., Menke, J. G., Kodali, S., Galgoci, A., Wang, J., and Singh, S. B. (2005) Anthrabenzoxocinones from Streptomyces sp. as liver X receptor ligands and antibacterial Agents. *J. Nat. Prod. 68*, 1437−1440.

(6) Chen, H., Liu, N., Huang, Y., and Chen, Y. (2014) Isolation of an anthrabenzoxocinone 1.264-C from Streptomyces sp. FXJ1.264 and absolute configuration determination of the anthrabenzoxocinones. *Tetrahedron: Asymmetry 25*, 113−116.

(7) Lü, Y., Shao, M., Wang, Y., Qian, S., Wang, M., Wang, Y., Li, X., Bao, Y., Deng, C., Yue, C., Liu, D., Liu, N., Liu, M., Huang, Y., Chen, Z., and Hu, Y. (2017) Zunyimycins B and C, new chloroanthrabenzoxocinones antibiotics against methicillin-resistant Staphylococcus aureus and Enterococci from Streptomyces sp. FJS31−2. *Molecules 22*, 251.

(8) Lü, Y., Yue, C., Shao, M., Qian, S., Liu, N., Bao, Y., Wang, M., Liu, M., Li, X., Wang, Y., and Huang, Y. (2016) Molecular genetic characterization of an anthrabenzoxocinones gene cluster in Streptomyces sp. FJS31−2 for the biosynthesis of BE-24566B and zunyimycin Ale. *Molecules 21*, 711.

(9) Feng, Z., Chakraborty, D., Dewell, S. B., Reddy, B. V. B., and Brady, S. F. (2012) Environmental DNA-encoded antibiotics fasamycins A and B inhibit FabF in type II fatty acid biosynthesis. *J. Am. Chem. Soc. 134*, 2981−2987.

(10) Ishikawa, F., Sugimoto, H., and Kakeya, H. (2016) In vitro investigation of crosstalk between fatty acid and polyketide synthases in the andrimid biosynthetic assembly line. *ChemBioChem 17*, 2137−2142.

(11) Qin, Z., Munnoch, J. T., Devine, R., Holmes, N. A., Seipke, R. F., Wilkinson, K. A., Wilkinson, B., and Hutchings, M. I. (2017) Formicamycins, antibacterial polyketides produced by Streptomyces formicae isolated from African tetraponera plant-ants. *Chem. Sci. 8*, 3218−3227.

(12) Xu, Z., Schenk, A., and Hertweck, C. (2007) Molecular analysis of the benastatin biosynthetic pathway and genetic engineering of altered fatty acid−polyketide hybrids. *J. Am. Chem. Soc. 129*, 6022−6030.

(13) Feng, Z., Kallifidas, D., and Brady, S. F. (2011) Functional analysis of environmental DNA-derived type II polyketide synthases reveals structurally diverse secondary metabolites. *Proc. Natl. Acad. Sci. U. S. A. 108*, 12629−12634.

(14) Kallifidas, D., Kang, H.-S., and Brady, S. F. (2012) Tetarimycin A, an MRSA-active antibiotic identified through Induced expression of environmental DNA gene clusters. *J. Am. Chem. Soc. 134*, 19552−19555.

(15) Sambrook, J., and Russell, D. W. (2001) *Molecular Cloning: A Laboratory Manual*, 3rd ed., Cold Spring Harbor Laboratory Press, New York.

(16) Kieser, T., Bibb, M., Butter, M., Chater, K. F., and Hopwood, D. A. (2001) *Practical Streptomyces Genetics*, The John Innes Foundation, Norwich, England.

(17) Zhang, B., Tian, W., Wang, S., Yan, X., Jia, X., Pierens, G. K., Chen, W., Ma, H., Deng, Z., and Qu, X. (2017) Activation of natural products biosynthetic pathways via a protein modification level regulation. *ACS Chem. Biol. 12*, 1732−1736.

DOI: 10.1021/acschembio.7b00743
ACS Chem. Biol. 2018, 13, 200−206